Nuclear Physics from Lattice QCD at Strong Coupling

Ph. de Forcrand[1,2] and M. Fromm[1]

[1]*Institute for Theoretical Physics, ETH Zürich, CH-8093 Zürich, Switzerland*
[2]*CERN, Physics Department, TH Unit, CH-1211 Geneva 23, Switzerland*

We study numerically the strong coupling limit of lattice QCD with one flavor of massless staggered quarks. We determine the complete phase diagram as a function of temperature and chemical potential, including a tricritical point. We clarify the nature of the low temperature dense phase, which is strongly bound "nuclear" matter. This strong binding is explained by the nuclear potential, which we measure. Finally, we determine, from this first-principles limiting case of QCD, the masses of "atomic nuclei" up to $A = 12$ "carbon".

It has been a long-standing goal to determine the properties of nuclear matter from first principles, using the theory which describes the interactions inside each nucleon, namely, quantum chromodynamics (QCD). Lattice QCD simulations have been extremely successful at determining the properties of a single proton, neutron or other hadron [1], and should in principle be appropriate for studying nuclear matter as well. Great progress has been made in this area, with the study of nuclear scattering lengths and potentials [2–4], and of the energies of two- and three-baryon systems [5]. Nevertheless, in these pioneering studies the quark masses are still far from their real-world values and the matter density is still very small. The *ab initio* study of real-world nuclear matter remains a distant goal. The technical issue of simulating quarks which are as light as in nature is being resolved [6], but two more obstacles stand in the way. (i) There is a large scale separation $\mathcal{O}(50)$ between the nucleons' masses and their binding energy. Accuracy on the latter requires excellent control over errors. (ii) There is a severe "sign problem": the functional integral at nonzero nuclear density has an oscillatory integrand, which causes large numerical cancellations and altogether prevents its usual interpretation as a Monte Carlo sampling probability. For these two reasons, the state-of-the-art approach is that of effective field theory [7], whose couplings still need to be derived by matching to QCD.

Here, we consider a limit of lattice QCD where the above obstacles can be overcome: the limit of infinite coupling. Because of asymptotic freedom, the lattice spacing a goes to zero with the bare coupling g as $a \propto \exp(-\frac{4\pi^2}{33}\beta)$ with $\beta = 6/g^2$. In the opposite limit $\beta = 0$ we will clearly have large lattice artifacts. Moreover, different discretizations of continuum QCD, all equivalent at weak coupling $\beta \gg 1$, may behave differently. We choose the staggered discretization of the Dirac operator and study the Euclidean partition function

$$Z(m_q, \mu) = \int \mathcal{D}U \mathcal{D}\bar{\chi}\mathcal{D}\chi e^{S_F}, \qquad (1)$$

with gauge links U in $SU(3)$ and action

$$S_F = \sum_{x,\nu=1,4} \eta_{x,\hat{\nu}}\bar{\chi}_x[U_{x,\hat{\nu}}\chi_{x+\hat{\nu}} - U^\dagger_{x-\hat{\nu},\hat{\nu}}\chi_{x-\hat{\nu}}]$$
$$+ 2m_q\sum_x \bar{\chi}_x\chi_x \qquad (2)$$

on a four-dimensional $N_s^3 \times N_\tau$ lattice, with antiperiodic boundary conditions in Euclidean time for the fermions χ, periodic otherwise. The $\eta_{x,\hat{\nu}} = (-1)^{\Sigma_{\rho<\nu}x_\rho}$, $\eta_{x,\hat{1}} = 1$ are the usual staggered phases. The chemical potential μ and an anisotropy γ are introduced by multiplying the timelike gauge links $U_{x,\pm\hat{4}}$ by $\gamma\exp(\pm a\mu/\gamma)$ in the forward and backward directions, respectively. The usual plaquette term which accounts for the gluonic action is absent here, since it is multiplied by β. The anisotropy γ allows the temperature T to be varied continuously, via $T = a^{-1}\gamma^2/N_\tau$ at infinite coupling [8]. In this Letter, we consider only one quark species and set its mass m_q to zero.

Our model is clearly very far from continuum QCD which contains two light quark flavors: our "quarks" live on a coarse cubic crystal, come in only one flavor and have no spin. This causes considerable changes in the symmetries of the theory, its bound states and their interactions, and its phase diagram. Our model belongs to the family of strongly correlated fermion systems rather than that of quantum field theories. Still, there is ample motivation to pursue its study. First, like continuum QCD, it confines colored objects, and has, for $m_q = 0$, a continuous global $U(1)$ symmetry

$$\chi(x) \rightarrow e^{i\varepsilon(x)\alpha}\chi(x), \qquad \bar{\chi}(x) \rightarrow \bar{\chi}(x)e^{i\varepsilon(x)\alpha} \quad \forall\ x, \quad (3)$$

where $\varepsilon(x) = (-1)^{\Sigma_\nu x_\nu}$. This is the 1-flavor version of chiral symmetry, spontaneously broken in the vacuum and restored at high temperature or density. Second, this model has been the object of analytic mean-field treatment since the earliest days of lattice QCD [9] continuing up to now [10–12]. These approximate analytic predictions should be checked against numerical simulations using an exact algorithm. Finally, all the obstacles for large β

mentioned earlier can be tamed by exploiting an alternative strategy, practical when $\beta = 0$.

Instead of performing the Grassmann integral in Eq. (1) and obtaining a determinant which becomes a complex function of the gauge links U when $\mu \neq 0$, one integrates analytically over the gauge links first [13]. After this step, only colorless objects survive and propagate from one lattice site to a neighboring site: mesons (pions), represented by unoriented ''dimers'' joining the two sites, and baryons, represented by oriented triple bonds. Because each site hosts $N_c = 3$ Grassmann fields χ and 3 fields $\bar{\chi}$, a triality constraint arises: each site is attached to exactly 3 dimers, or is traversed by a baryon loop. Thus, baryon loops are self-avoiding. After performing the Grassmann integration, the partition function becomes a weighted sum over configurations of dimers ($n_{x,\hat{\nu}} = 0, \ldots, 3$ dimers for each link $x, \hat{\nu}$) and self-avoiding baryon loops C [14]:

$$Z(\mu) = \sum_{\{n_{x,\hat{\nu}},C\}} \prod_{x,\hat{\nu}} \gamma^{2\delta_{\nu,4}n_{x,\hat{4}}} \frac{(3 - n_{x,\hat{\nu}})!}{n_{x,\hat{\nu}}!} \prod_C w(C), \quad (4)$$

where a weight $w(C) = \rho(C)\gamma^{3N_{\hat{4}}(C)} \exp(3k\mu aN_\tau/\gamma)$ is associated with each baryon loop C. Here, $N_{\hat{4}}(C)$ is the number of timelike links on the loop, k is its winding number in this direction and $\rho(C) = \pm 1$ is a geometry-dependent sign. Thus, the weight of a configuration can be negative even when $\mu = 0$, which seems much worse than the traditional strategy. Yet, this sign problem can be solved by analytically resumming configurations where C is a baryon loop or a self-avoiding pion loop made of alternating single and double dimers [14]. After this step, the sign problem remains mild even when $\mu \neq 0$ [15], so that lattices of size $16^3 \times 4$ can be simulated using the standard technique of reweighting at all values of μ, thus allowing for a reliable determination of the full (μ, T) phase diagram. The final technical difficulty is to devise a Monte Carlo algorithm which preserves the triality constraint at each site. This is achieved by the worm algorithm [16], adapted for strong coupling $SU(2)$ and $U(3)$ lattice theories in [17], and readily modified here for $SU(3)$. It produces global updates whose high efficiency does not degrade as $m_q \to 0$.

Setting the scale.—We first compared, at $T = \mu = 0$ and for nonzero quark mass, the results of our approach with those of the traditional sampling of the fermion determinant with the Hybrid Monte Carlo algorithm on the same $8^3 \times 16$ lattice size [18]: there was complete agreement. Then, setting $m_q = 0$, we extracted the baryon mass m_B from its Euclidean correlator $G(\tau)$, obtaining $am_B = -1/2 \log G(\tau + 2a)/G(\tau) = 2.88(1)$, in close agreement with mean-field [9] and large-N_c [19] predictions. Equating our baryon mass with the real-world proton mass gives $a \approx 0.63$ fm. Using instead the Δ mass, which is perhaps more appropriate for our one-flavor model, gives $a \approx 0.46$ fm. Alternatively, from the ρ meson mass and the pion decay constant we obtain $a \approx 0.455$ fm and $a \approx$

1.4 fm, respectively. These different values give us an estimate of the effective coarseness of our lattice, and their dispersion gives an idea of the magnitude of our systematic errors when comparing to real-world QCD: our model is only a caricature of the latter.

Phase diagram.—We now turn to the phase diagram as a function of temperature T and quark chemical potential μ [15]. Since we take the quark mass to vanish, the chiral symmetry Eq. (3) is exact but spontaneously broken at small (μ, T), with order parameter $\langle \bar{\psi}\psi \rangle$. When $\mu = 0$, a mean-field analysis predicts symmetry restoration at $aT_c = 5/3$, whereas the Monte Carlo study of [20] on $N_\tau = 4$ lattices, extrapolated to $m_q = 0$, finds $aT_c = 1.41(3)$. Here, simulating directly at $m_q = 0$, we assume critical exponents of the expected $3d$ $O(2)$ universality class, and find $aT_c = 1.319(2), 1.402(3), 1.417(3)$, respectively, for $N_\tau = 2, 4, 6$, indicating an $N_\tau \to \infty$ limit about 15% smaller than the mean-field prediction. At $T = 0$ the transition is strongly first order, as we will see shortly. A tricritical point separates the regimes of first- and second-order transitions. Using finite-size scaling on $N_\tau = 4$ lattices, we determine its location to be $(a\mu_{\text{TCP}}, aT_{\text{TCP}}) = (0.33(3), 0.94(7))$ (see Fig. 1). This should be compared with the analytic prediction (0.577, 0.866) of [11]. The rather large difference in μ_{TCP} underlines the $\mathcal{O}(1/d)$ accuracy of a mean-field treatment, and justifies *a posteriori* our Monte Carlo study.

In spite of the resemblance of Fig. 1 to the expected deconfinement transition in massless two-flavor QCD, here the two phases are both confining, with pointlike mesons and baryons, and so the phase transition is to dense, chirally symmetric, crystalline nuclear matter. At $T = 0$ the baryon density jumps from 0 to 1, a saturation value caused by the self-avoiding nature of the baryon loops, which itself originates from their fermion content. In physical units, this represents about 4 ''nucleons'' per fm^3, around 25 times the real-world value.

An intriguing feature of this $T = 0$ transition is the value of μ^{critical}, which both mean-field [9] and an early Monte Carlo study [14] find much smaller than the naive threshold value $m_B/3$. However, the ergodicity of the
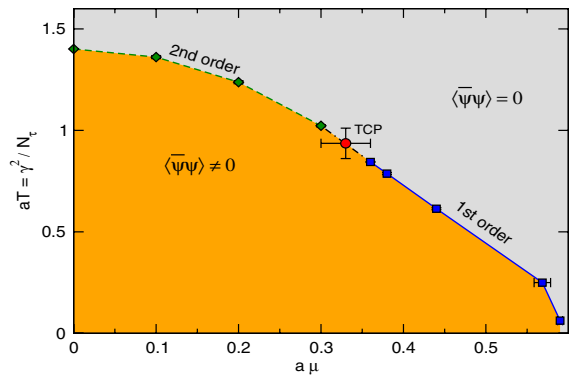

FIG. 1 (color online). (μ, T) phase diagram of 1-flavor strong coupling QCD, with massless staggered fermions ($N_\tau = 4$).

simulations of [14] was questioned in [21], which was found to be justified in [22]. This motivated us to redetermine $\mu^{\mathrm{crit}}(T = 0)$ using an improved method inspired by the "snake" algorithm [23]: When two phases coexist, the free energy necessary to increase by a "slice" $L \times L \times a$ the volume occupied by dense nuclear matter can be decomposed into L^2 elementary contributions, looking generically like Fig. 2(a), where one additional static baryon is attached to 3 neighbors. We measured the free energy $\Delta F/T$ of this elementary increment on a large $8^3 \times 16$ lattice, and obtained $a\Delta F = a\mu_B^{\mathrm{crit}} = 1.78(1)$, rather close to both mean-field predictions [9] and Monte Carlo extrapolations [14], but much smaller than am_B. As already recognized in [24], the reason that $\mu_B^{\mathrm{crit}} < m_B$ must then be the presence of a strong nuclear attraction.

Nuclear matter.—Since our baryons are pointlike, there is no conceptual difficulty in defining the nuclear potential $V_{\mathrm{NN}}(R)$, unlike in the real world [25]. We measured V_{NN} using again the snake algorithm, this time extending little by little in Euclidean time the worldline of a second baryon at distance R from the first. The result is shown in Fig. 3. Aside from the hard-core repulsion, there is indeed a strong nearest-neighbor attraction, a slight repulsion at distance $a\sqrt{2}$, and almost no interaction beyond that distance. Thus, V_{NN} has similar features to the real-world nuclear interaction, whose properties are commonly ascribed to subtle competition between attractive σ exchange and repulsive ω exchange. The depth of the minimum ~ 120 MeV and the corresponding distance ~ 0.6 fm are even quantitatively plausible. This nearest-neighbor attraction also explains *a posteriori* the value of μ_B^{crit}: each baryon added to the dense phase binds with 3 nearest neighbors, which reduces the increase in free energy from am_B to only $a(m_B + 3V_{\mathrm{NN}}(a)) \approx 1.7$, consistent with $a\mu_B^{\mathrm{crit}}$.

Similarly, we can predict the $T = 0$ surface tension of nuclear matter: in a periodic cubic box, when building a first slice of nuclear matter with two interfaces in the dilute phase, each new baryon binds with only 2 nearest neighbors [Fig. 2(b)] instead of 3 in the bulk [Fig. 2(a)], thus increasing its free energy by $|V_{\mathrm{NN}}(a)|$ for an increase of $2a^2$ in the interface area, yielding $\sigma \approx \frac{a^{-2}}{2}|V_{\mathrm{NN}}(a)|$.

This large interface tension ~ 200 MeV/fm^2 has an impact on the stability of "nuclei" of various sizes and

shapes: for a given atomic number A, those with a shape close to a sphere (or a cube) will have a smaller mass. Using the same variant of the snake algorithm, we have added baryons, one by one, to form such nuclei while measuring the successive increments in free energy. For $A = 2$ our "deuteron" binding energy is about 120 MeV: the real-world binding energy of ~ 2 MeV results from delicate cancellations which do not occur in our 1-flavor model, and the binding energy remains of the same magnitude as the depth of V_{NN}. For larger A, the resulting Fig. 4(a) does indeed show increased stability for nuclei having square ($A = 4$), cubic ($A = 8$) or parallelepipedic ($A = 12$) shapes. Other "isomers" with different shapes, studied exhaustively for $A = 4$ and sketched in Fig. 4(b), have clearly larger masses. Moreover, the average mass per "nucleon" is well described by the first two (bulk and surface tension) terms of the Weizsäcker phenomenological formula:

$$m(A)/A = \mu_B^{\mathrm{crit}} + (36\pi)^{1/3}a^2\sigma A^{-1/3}, \qquad (5)$$

where σ is set equal to $\frac{a^{-2}}{2}|V_{\mathrm{NN}}(a)|$ in the figure. The next higher-order terms in this formula come from isospin and Coulomb forces, which are both absent in our model.

Discussion and Conclusions.—An interesting aspect of our study is the *origin* of the nuclear interaction. The nucleons are pointlike and self-avoiding, so that only the hard-core repulsion is explicit. There is no direct meson exchange in our crude model. In a way reminiscent of the Casimir effect between two neutral plates, the interaction proceeds by the rearrangement of the pion bath caused by the excluded volume of the nucleon. This rearrangement is visible in Fig. 5 for one nucleon: at a neighboring site, the three pion lines attached to each site have fewer options and orient more often along the Euclidean time, which increases the pion energy. In fact, the nucleon mass $am_B \approx 2.88$ can be decomposed into a bare mass $3 - 3/4 = 2.25$, which is the energy increase "inside" the nucleon and can be assigned to the three valence quarks, and an energy
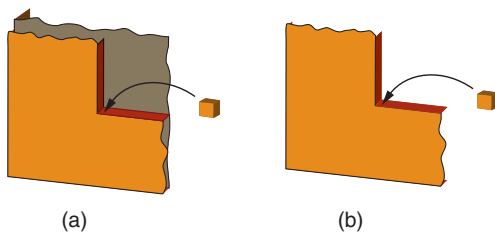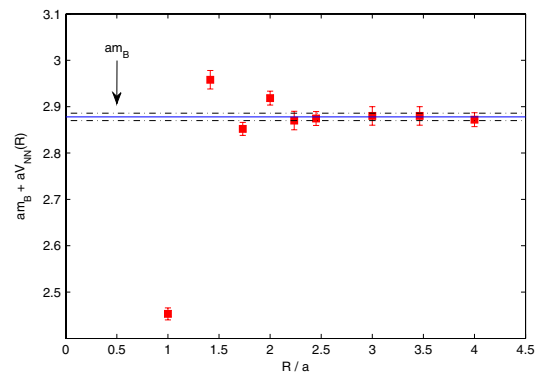

FIG. 2 (color online). (a) Adding a baryon to grow an additional layer of bulk nuclear matter. Each new baryon binds to 3 nearest neighbors. (b) Building a first layer of nuclear matter inside the hadron gas, thus creating two interfaces. Each new baryon binds to 2 nearest neighbors.

FIG. 3 (color online). Energy of a second static baryon at distance R from the first, i.e., $[m_B + V_{\mathrm{NN}}(R)]$, where $V_{\mathrm{NN}}(R)$ is the nuclear interaction potential. The horizontal band indicates the mass of an isolated baryon and corresponds to $V_{\mathrm{NN}} = 0$. At $R = 0$ the potential is infinitely repulsive.
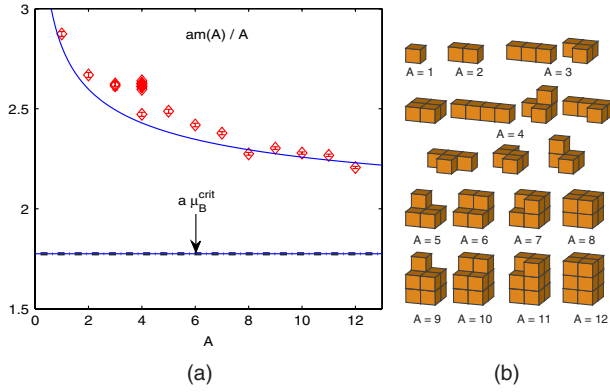
FIG. 4 (color online).   (a) Mass per nucleon of $A = 1, \ldots, 12$ nuclei. For $A = 3, 4$ all possible geometric isomers are included. The solid line shows the parameter-free Bethe-Weizsäcker Eq. (5), with the surface tension σ set to $\frac{a^{-2}}{2}|V_{NN}(a)|$. (b) Corresponding nuclear geometries in order of increasing mass.

increase ≈ 0.63 in the surrounding pion "cloud". When two nucleons are next to each other, the latter increase is limited to 10 nearest neighbors instead of 2×6, which explains the attraction between them (in sign and roughly in magnitude). This excluded volume or *steric* effect is thus the origin of the nuclear potential, and ultimately of nuclear stability, in our model. In real QCD, the pion density is not constrained as in Eq. (4). Nevertheless, it is going to be high at temperatures $T \sim m_\pi$ [26] and one should expect the same steric effect to enhance nuclear attraction at such temperatures.

To summarize, in a crude model of QCD, 1-flavor lattice staggered fermions at strong coupling $\beta = 0$, we have been able to obtain the (μ, T) phase diagram and derive nuclear interactions and nuclear masses from first principles, uncovering a simple, but universal, steric origin of the nuclear interaction. This model can be improved in many ways. One simple modification consists of giving a nonzero mass to the quarks: the nuclear interaction will weaken as the pion mass is increased, in a way which can be compared with effective field theories. Less simple but feasible improvements include introducing isospin with a second quark flavor, and measuring the $\mathcal{O}(\beta)$ correction as
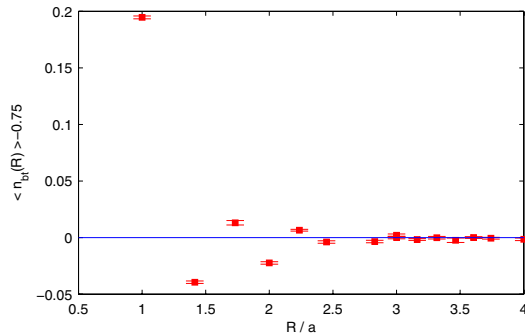
done analytically in [27,28]. These will bring our model much closer to real QCD.

[1] S. Dürr *et al.*, Science **322**, 1224 (2008).
[2] S. R. Beane, P. F. Bedaque, K. Orginos, and M. J. Savage, Phys. Rev. Lett. **97**, 012001 (2006); S. R. Beane, K. Orginos, and M. J. Savage, Int. J. Mod. Phys. E **17**, 1157 (2008).
[3] N. Ishii, S. Aoki, and T. Hatsuda, Mod. Phys. Lett. A **23**, 2281 (2008).
[4] A. Gardestig, J. Phys. G **36**, 053001 (2009).
[5] S. R. Beane *et al.*, Phys. Rev. D **80**, 074501 (2009).
[6] K. Jansen, Proc. Sci., LAT2008 (2008) 010; L. Giusti, Proc. Sci., LAT2006 (2006) 009; M. Lüscher, Proc. Sci., LAT2005, (2006) 002.
[7] E. Epelbaum, H. W. Hammer, and U. G. Meissner, Rev. Mod. Phys. **81**, 1773 (2009); W. Weise, Nucl. Phys. A **805**, 115c (2008); D. B. Kaplan, arXiv:nucl-th/0510023.
[8] P. H. Damgaard, N. Kawamoto, and K. Shigemoto, Nucl. Phys. B **264**, 1 (1986).
[9] J. Hoek, N. Kawamoto, and J. Smit, Nucl. Phys. B **199**, 495 (1982); H. Kluberg-Stern, A. Morel, and B. Petersson, Nucl. Phys. B **215**, 527 (1983).
[10] N. Kawamoto, K. Miura, and A. Ohnishi, Proc. Sci. LAT2007 (2007) 209.
[11] Y. Nishida, Phys. Rev. D **69**, 094501 (2004).
[12] K. Miura and A. Ohnishi, Prog. Theor. Phys. **122**, 1045 (2009).
[13] P. Rossi and U. Wolff, Nucl. Phys. B **248**, 105 (1984).
[14] F. Karsch and K. H. Mütter, Nucl. Phys. B **313**, 541 (1989).
[15] M. Fromm and P. de Forcrand, arXiv:0912.2524.
[16] N. Prokof'ev and B. Svistunov, Phys. Rev. Lett. **87**, 160601 (2001).
[17] D. H. Adams and S. Chandrasekharan, Nucl. Phys. B **662**, 220 (2003); S. Chandrasekharan and F. J. Jiang, Phys. Rev. D **74**, 014506 (2006).
[18] P. de Forcrand and S. Kim, Phys. Lett. B **645**, 339 (2007).
[19] O. Martin, Phys. Lett. B **130**, 411 (1983).
[20] G. Boyd *et al.*, Nucl. Phys. B **376**, 199 (1992).
[21] R. Aloisio *et al.*, Nucl. Phys. B **564**, 489 (2000).
[22] M. Fromm and P. de Forcrand, Proc. Sci., LAT2008 (2008) 191.
[23] P. de Forcrand, M. D'Elia, and M. Pepe, Phys. Rev. Lett. **86**, 1438 (2001); Nucl. Phys. B, Proc. Suppl. **94**, 494 (2001).
[24] N. Bilic, K. Demeterfi, and B. Petersson, Nucl. Phys. B **377**, 651 (1992).
[25] S. R. Beane, Proc. Sci., LAT2008 (2008) 008.
[26] P. Gerber and H. Leutwyler, Nucl. Phys. B **321**, 387 (1989).
[27] G. Faldt and B. Petersson, Nucl. Phys. B **265**, 197 (1986).
[28] N. Bilic, F. Karsch, and K. Redlich, Phys. Rev. D **45**, 3228 (1992).

FIG. 5 (color online).   Energy density of the pion cloud as a function of the Euclidean distance to a static baryon.